Journal of Applied Physics

RESEARCH ARTICLE | DECEMBER 09 2022

Exploiting plasmons in 2D metals for refractive index sensing: Simulation study

Lei Kang ; Joshua A. Robinson ; Douglas H. Werner

Journal of Applied Physics 132, 223103 (2022)
https://doi.org/10.1063/5.0123648

Journal of Applied Physics ARTICLE scitation.org/journal/jap

Exploiting plasmons in 2D metals for refractive index sensing: Simulation study

Cite as: J. Appl. Phys. **132**, 223103 (2022); doi: 10.1063/5.0123648
Submitted: 31 August 2022 · Accepted: 21 November 2022 ·
Published Online: 9 December 2022

Lei Kang,[1,a)] Joshua A. Robinson,[2] and Douglas H. Werner[1,b)]

AFFILIATIONS

[1]Department of Electrical Engineering and Center for Nanoscale Science, The Pennsylvania State University, University Park, Pennsylvania 16802, USA
[2]Department of Materials Science and Engineering, Department of Physics, Department of Chemistry, Center for Nanoscale Science, 2D Crystal Consortium, Center for Atomically Thin Multifunctional Coatings, and Center for 2D and Layered Materials, The Pennsylvania State University, University Park, Pennsylvania 16802, USA

[a)]**Author to whom correspondence should be addressed:** lzk12@psu.edu
[b)]**Electronic mail:** dhw@psu.edu

ABSTRACT

Ultrathin and two-dimensional (2D) metals can support strong plasmons, with concomitant tight field confinement and large field enhancement. Accordingly, 2D-metal nanostructures exhibiting plasmonic resonances are highly sensitive to the environment and intrinsically suitable for optical sensing. Here, based on a proof-of-concept numerical study, nano-engineered ultrathin 2D-metal films that support infrared plasmons are demonstrated to enable highly responsive refractive index (RI) sensing. For 3 nm-Au nanoribbons exhibiting plasmonic resonances at wavelengths around 1600 nm, a RI sensitivity of $S_{RI} > 650$ nm per refractive index unit (RIU) is observed for a 100 nm-thick analyte layer. A parametric study of the 2D-Au system indicates the strong dependence of the RI sensitivity on the 2D-metal thickness. Furthermore, for an analyte layer as thin as 1 nm, a RI sensitivity up to 110 (90 nm/RIU) is observed in atomically thin 2D-In (2D-Ga) nanoribbons exhibiting highly localized plasmonic resonances at mid-infrared wavelengths. Our results not only reveal the extraordinary sensing characteristics of 2D-metal systems but also provide insight into the development of 2D-metal-based plasmonic devices for enhanced IR detection.

I. INTRODUCTION

Optically induced collective oscillation of electrons at a metal/dielectric interface, referred to as surface plasmons (SPs), provides the basis for strong light-matter interaction on a nanometer scale. Given the fact that SPs are closely dependent on the degrees of freedom of electrons in responding to optical excitation, SPs in two-dimensional (2D) systems [such as graphene, transition metal dichalcogenides (TMDCs), etc.] behave differently than those seen at the surfaces of conventional metal films (e.g., thickness $t_M \geq 30$ nm).[1] The recent advances in growing atomically thin metal [e.g., gold (Au) and silver (Ag)] films make it possible to explore SPs supported by such ultrathin (or 2D) metal films. Abd El-Fattah *et al.* have demonstrated sharp plasmonic resonances in crystalline silver nanoribbons whose thicknesses were in the few atomic-layer range.[2] Maniyara and co-workers have shown that nanostructures based on ultrathin gold films can support electrical-gating tunable plasmons,[3] an attractive plasmonic behavior that was previously seen in graphene. It should be noted that because the carrier density in 2D-metals is typically orders of magnitude higher than that in graphene, 2D-metals are capable of supporting SPs in the near- and mid-infrared spectral range. Furthermore, by performing *ab initio* calculations, da Jornada *et al.* have theoretically predicted that 2D-metals can support universal slow plasmons accompanied by giant field enhancements.[4] Moreover, with the predicted reduced optical losses,[5–9] 2D-metals have also been demonstrated as a transformative platform for possessing quantum optical effects.[10,11] These superior properties indicate the potential of 2D-metals for an entire family of plasmonic devices capable of exhibiting enhanced functionalities in the infrared.

Among the characteristics of SPs, the plasmonic resonance induced field concentration is the key to light manipulation with subwavelength-scale localization. Strong field confinement in plasmonic nanostructures is not only associated with a series of intriguing optical phenomena in the linear regime, such as extraordinary transmission,[12,13] perfect absorption,[14,15] strong chirality,[16,17] etc., but also with a variety of enhanced nonlinearities.[18–20] Leveraging the enhanced optical field due to plasmon excitations in noble metal (e.g., Au) nanostructures, surface enhanced Raman spectroscopy (SERS), and surface enhanced fluorescence (SEF) have been widely used in the analysis of biochemical substances.[21–24] Furthermore, compared with SERS and SEF, periodic-structure-based plasmonic sensors for refractive index (RI) detection have also been extensively studied owing to their label-free characteristics together with the fact that they are more readily available. Indeed, the pronounced sensitivity in RI detection has made plasmonic sensors a powerful tool for analytical applications.[25,26] In the perturbation regime, the corresponding RI sensitivity (S_{RI}) is proportional to $\int_A \boldsymbol{E}_m^2 dV$, where $\boldsymbol{E}_m$ is the resonant field distribution and A represents the volume of the analyte region.[27] In other words, S_{RI} is simultaneously determined by the local-field concentration and the overlap of the field with the analyte. Considering the field confinement effect associated with plasmonic resonances in conventional nanostructures, an analyte (sensing) layer of a characteristic thickness (t_s) of hundreds of nanometers is generally required for optimal sensing performance in the near-infrared wavelength region. For instance, Weiss *et al.* have reported a maximum $S_{RI} \sim 700$ nm/RIU for a plasmonic sensor consisting of an Au nanodisk array ($t_{Au} = 30$ nm) for sensing volumes with a thickness (t_s) of 650 nm.[27] Although S_{RI} can be improved by exploiting the coupling between different plasmonic modes (for example, by creating Fano resonances),[28–32] the performance of the existing plasmonic sensors is intrinsically limited by the material properties of conventional metal films. On the other hand, due to the vanishing plasmons in most bulk metals at longer wavelengths, plasmonic sensors in the mid-infrared, which offer a series of beneficial aspects including less photodamage to bio-samples, the potential for vibrational spectroscopy of molecules, etc., are still rare.[33–35] Therefore, plasmonic sensors, which require significantly less amount of analyte and are capable of operating in the mid-infrared are highly desirable. To this end, 2D-material sensors have been intensively studied due to the high degree of sensitivity in the properties of 2D materials (such as graphene, 2D chalcogenides, etc.) to external stimuli.[36–41] Here, we focus on plasmonic sensors based on 2D-metals, which are considered an emerging material family with a wide array of potential applications.

Compared with conventional metal films, 2D-metals exhibit strong plasmonic energy dispersion due to the thickness effect, leading to the extreme field confinement as well as a significant increase in the local-field enhancement factor. These properties indicate that 2D-metals might be a promising material system for optical sensing applications. In this work, by performing a proof-of-concept study, we numerically demonstrate refractive index detection based on 2D-metal nanostructures. Our simulations are based on measured material properties of 2D-Au, 2D gallium (Ga), and 2D indium (In).[3,42] Our results show that the RI sensitivity of the 2D-metal sensors dramatically increases with decreasing thickness of the plasmonic structures. Furthermore, the atomically thin 2D-In (2D-Ga) nanostructures, which support highly localized plasmonic resonances at mid-infrared wavelengths, exhibit a RI sensitivity of 110 (90 nm/RIU) for an analyte thickness of 1 nm. Our study reveals that the atomistic local-field effects associated with the intrinsic dispersion property of 2D-metals can substantially enhance the sensitivity of plasmonic sensors in the near- and mid-infrared regions, which suggests a new family of 2D-metal-based plasmonic devices for enhanced infrared detection.

II. RESULTS

As illustrated in Fig. 1(a), we first consider a periodic 2D-Au nanoribbon array ($t_{Au} = 3$ nm) located on top of an infrared-transparent CaF_2 substrate ($\varepsilon_{CaF2} = 2.03$),[3] which has a conformal cover layer (of thickness t_s) that serves as the sensing volume (analyte) with a refractive index n_s. Here, we utilize thickness-dependent representations of the 2D-Au film permittivities to describe their plasmonic properties due to the thickness effect (see the supplementary material for details). The system is illuminated by a plane wave with the electric field oriented across the width of the nanoribbons. To evaluate the optical response of the 2D-Au nanoribbons and the corresponding spectral shift in relation to the variations in n_s and t_s, we performed full-wave simulations using the commercial finite integration package CST Microwave Studio. Figure 1(b) shows the simulated transmittance spectra at normal incidence when n_s of a 10 nm-thick analyte layer increases from 1.25 to 1.55, indicating a pronounced redshift of the resonance. For comparison purposes, a (conventional) RI sensing system based on Au nanoribbons of the same geometry but $t_{Au} = 30$ nm was also studied, for which the corresponding transmittance spectra [Fig. 1(b)] reveal a trivial spectral variation compared with the 3-nm-Au system. This difference primarily arises from the distinct field confinement behavior of the two systems. The on-resonance electric field distribution of the 3 nm-Au system [Fig. 1(c)] indicates a strongly localized optical mode, which gives rise to an up to 20-fold field enhancement in the close vicinity of the nanoribbons. In contrast, only weak field confinement is found in the 30 nm-Au system. The evaluation of $|E|dx$ in a unit cell [Fig. 1(e)] unambiguously shows the Au-thickness-dependent field enhancement effect. In particular, the steep growth in the strong field at the air/3 nm-Au interface, as studied by Maniyara and co-workers,[3] suggests that the 2D-Au sensors possess an inherently higher degree of sensitivity.

The spectral shift of plasmonic resonances is determined by a change in both n_s and t_s of the analyte layer and can be expressed as $\Delta\lambda = \left(\frac{\partial\lambda}{\partial n_s}\right)\Delta n_s + \left(\frac{\partial\lambda}{\partial t_s}\right)\Delta t_s$.[43] We show in Fig. 1(f) the resonance wavelength change ($\Delta\lambda$) for both systems as a function of n_s in the sensing volume when t_s varies from 2 to 10 nm. It can be seen that, for a certain t_s, $\Delta\lambda$ of both systems displays an approximately linear dependence on the n_s, while, for a fixed refractive index change (e.g., $\Delta n_s = 1.55–1.25$), $\Delta\lambda$ of the 3 nm-Au system shows a significantly larger increase than the 30-nm-Au nanoribbons. In addition to $\Delta\lambda$, the resonance linewidth (defined by the full width at half maximum (FWHM) of the transmittance spectra in our study) associated with $-2\mathrm{Im}(\omega_m)$, where ω_m is the complex eigenfrequency of the plasmonic resonance, also represents an important

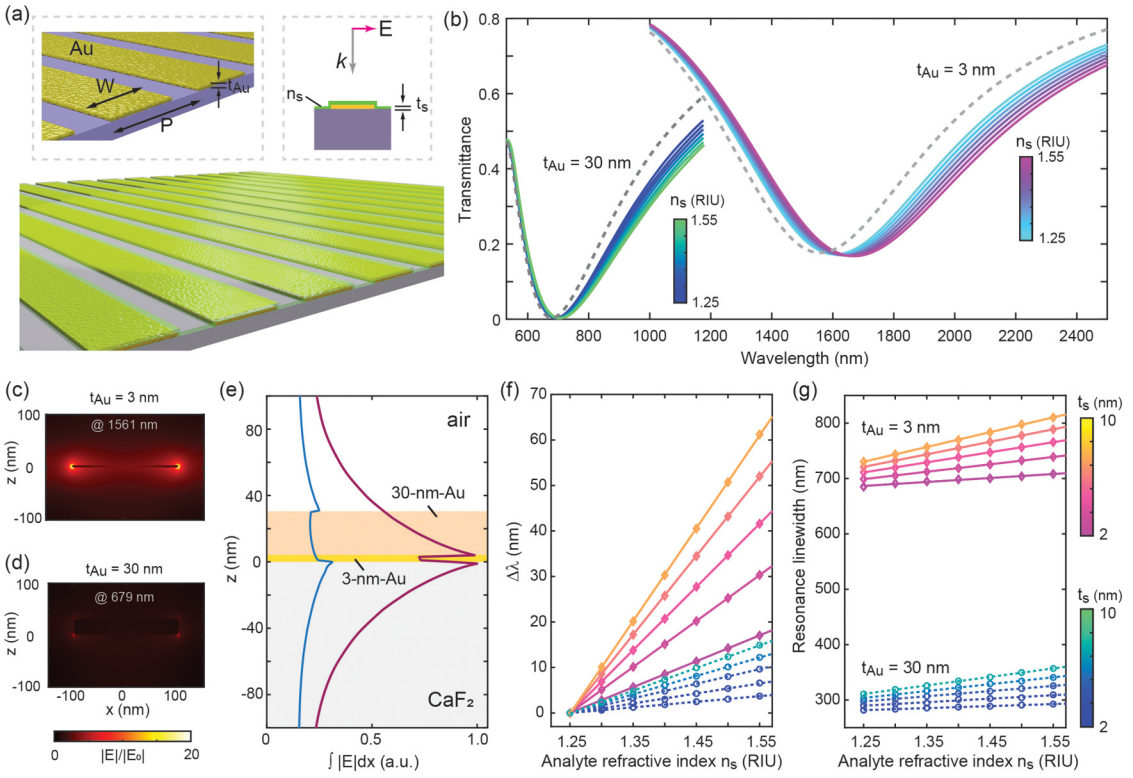

FIG. 1. Refractive index sensing based on infrared plasmons in ultrathin metals. (a) Schematic of the sensor consisting of an array of ultrathin gold nanoribbon structures located on a CaF_2 substrate. The device is coated with an analyte (refractive index, n_s) with a thickness of t_s. Geometry: $W = 200$ nm, $P = 1.5W$, and $t_{Au} = 3$ nm. (b) Transmittance spectra at normal incidence when n_s varies and $t_s = 10$ nm. For comparison, the transmittance spectra of a (conventional) system of the same geometry but with $t_{Au} = 30$ nm are also presented. Spectra of both systems without the analyte coating are shown as dashed curves. The corresponding electric field distributions on the cross-sectional plane at a resonance wavelength of (c) 1561 and (d) 679 nm. The electric field magnitude is normalized to that of the incident wave. In addition, to minimizing the substrate effect, the electric field obtained from the same unit cell without the nanoribbons was subtracted from the total field. (e) Normalized $|E|dx$ in a unit cell representing the field enhancement effect in the z direction (normal to the devices' surface). (f) The resonance wavelength change ($\Delta\lambda$) and (g) resonance linewidth as a function of n_s for both systems for a series of t_s. Markers in (f) and (g) are simulated results, while the curves are included as fits to the discrete data points.

figure of merit (FOM) for the sensors.[27] A combination of the RI sensitivity ($\partial\lambda/\partial n$) and resonance linewidth provides a comprehensive description of the FOM of the proposed sensors. As illustrated in Fig. 1(g), the linewidth increases monotonically with n_s and t_s in the studied range. We note that, compared with that of the conventional Au nanoribbons, the relatively large resonance linewidth of the 3-nm-Au system can be attributed to an increase in material loss (see the supplementary material for details).

To provide a complete picture of the 3 nm-Au sensor's performance, we further study its sensitivity and summarize the results in Fig. 2. Note that, as the insets in Fig. 2(a) depict, based on the geometry of the nanoribbons the results can be divided into either conformal ($t_s < 50$ nm) or nonconformal ($t_s \geq 50$ nm) regions. Figure 2(a) shows an increasing resonance wavelength shift $\Delta\lambda$ corresponding to an increasing t_s for $\Delta n_s = 1.50–1.40$, which determines the dependence of the RI sensitivity $\partial\lambda/\partial n$ on t_s shown in Fig. 2(b). A RI sensitivity $\partial\lambda/\partial n = 655$ nm/RIU is observed at $t_s = 100$ nm, which is comparable with that found in previously reported conventional plasmonic sensor based Au nanostructures covered by a micrometer-thick analyte.[27,32] The thickness sensitivity $\partial\lambda/\partial t$ [Fig. 2(c)], which corresponds to the resonance wavelength change solely due to the variation in t_s, better reflects the strong field confinement at the interface of the ultrathin Au film. In particular, for $t_s = 1$ nm, the observed $\partial\lambda/\partial t = 11$ nm/nm is more than 20 times larger than that seen in conventional RI sensor based 2D photonic crystal slabs.[44] The trend observed in Figs. 2(a)–2(c) suggests a saturation analyte thickness around 100 nm, while, in contrast, the resonance linewidth increases with increasing t_s but becomes invariant when $t_s > 50$ nm.

To better understand the thickness-dependent capability of ultrathin metals for RI sensing, we further study the nanoribbon systems with $t_{Au} = 6$ and 15 nm. The thickness-dependent material property of ultrathin Au films was used in the simulations. For comparison purposes, the results are shown in Fig. 3 along with the systems with $t_{Au} = 3$ and 30 nm (see the supplementary material for the complete simulation data set including the transmittance

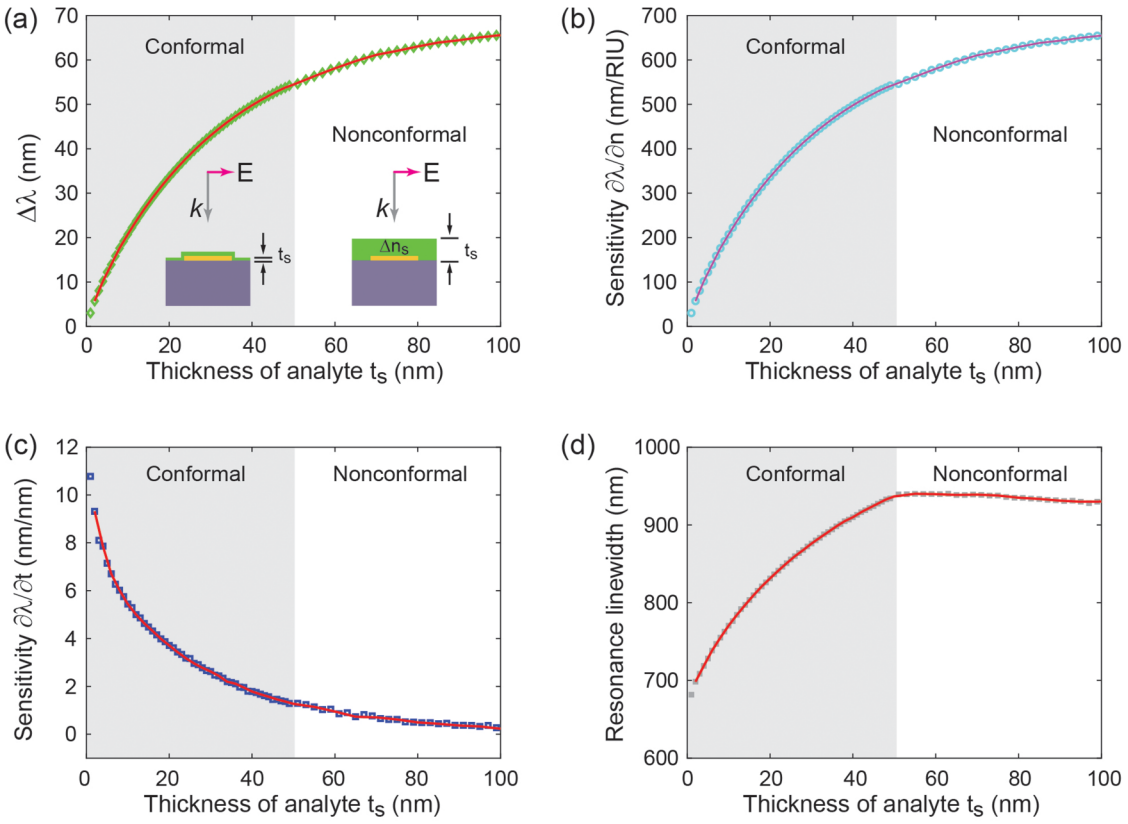

FIG. 2. Sensitivity study of the sensor based on 3 nm-Au nanoribbons. The dependence of (a) the resonance wavelength shift ($\Delta\lambda$) when $\Delta n_s = 1.50$–1.40, (b) RI sensitivity $\partial\lambda/\partial n$, (c) thickness sensitivity $\partial\lambda/\partial t$ ($n_s = 1.40$), and (d) resonance linewidth on the thickness of the analyte (t_s). The geometry of the systems is the same as those shown in Fig. 1. As depicted in the insets in (a), the analyte layer is considered as a conformal (nonconformal) coating when $t_s < 50$ nm ($t_s \geq 50$ nm). In all panels, the markers represent the simulated results, and the solid curves are included as fits to the discrete data points.

spectra). The transmittance spectra shown in Fig. 3(a) indicate the plasmonic resonances supported by each system. In particular, the inset of Fig. 3(a) indicates the nonlinear dependence of the normalized wavenumber of the resonances ($k_{norm} = \lambda_{res}/P$) on t_{Au}. Figures 3(b), 3(d), and 3(f) summarize the dependences of $\Delta\lambda$ on n_s for the four systems when $t_s = 2$, 6, and 10 nm, respectively, while Figs. 3(c), 3(e), and 3(g) show the corresponding resonance linewidth results. Clearly, the 3 nm-Au system exhibits superior RI sensitivity compared to the other systems that are based on thicker Au films, with a concomitant increase in the resonance linewidth. It is notable that, compared with the conventional (30 nm-Au) system, 15 nm-Au shows a comparable (even lower) RI sensitivity but a larger resonance linewidth. This can be attributed to the larger material loss of the 15 nm-Au, which restricts the thickness-induced dispersion effect (λ_{res}/P for 15 nm-Au nanoribbons is slightly higher than that of the 30 nm-Au system; see the supplementary material for a comparison of the simulated field distributions). These results suggest that creating highly sensitive 2D-metal-based RI devices requires ultrathin metals (only a few nanometers thick) that are capable of supporting strong plasmons in the infrared region.

The recent development of confinement heteroepitaxy (CHet), based on intercalation of metallic elements at the graphene/SiC interface,[45] provides a new opportunity for the synthesis of large-area atomically thin 2D polar metals with precisely controlled thickness (number of atomic metal layers). More importantly, protected by epitaxially grown graphene, 2D polar metals realized by the CHet process are suitable for nanopatterning and, therefore, are good candidates for plasmonic devices.[46] The optical properties of 2D-Ga and 2D-In in the linear regime and their extremely large second-order susceptibilities have been reported recently.[42,47] In particular, the measured permittivity dispersions of 2D-Ga and 2D-In indicate plasmon frequencies in the near-IR region, which suggests that these two material systems can be utilized to achieve plasmonic responses in the near- to mid-infrared spectral range. Here, we consider RI sensors based on bilayer (2L) 2D-Ga and 2D-In with dielectric properties reported in previous studies.[42] Schematics in the inset of Figs. 4(a) and 4(b) display the unit cell of the studied systems: a graphene-covered 2D-metal nanoribbon located on top of a silicon carbide (SiC) substrate, which is covered by a conformal analyte layer. In our simulations, for simplicity,

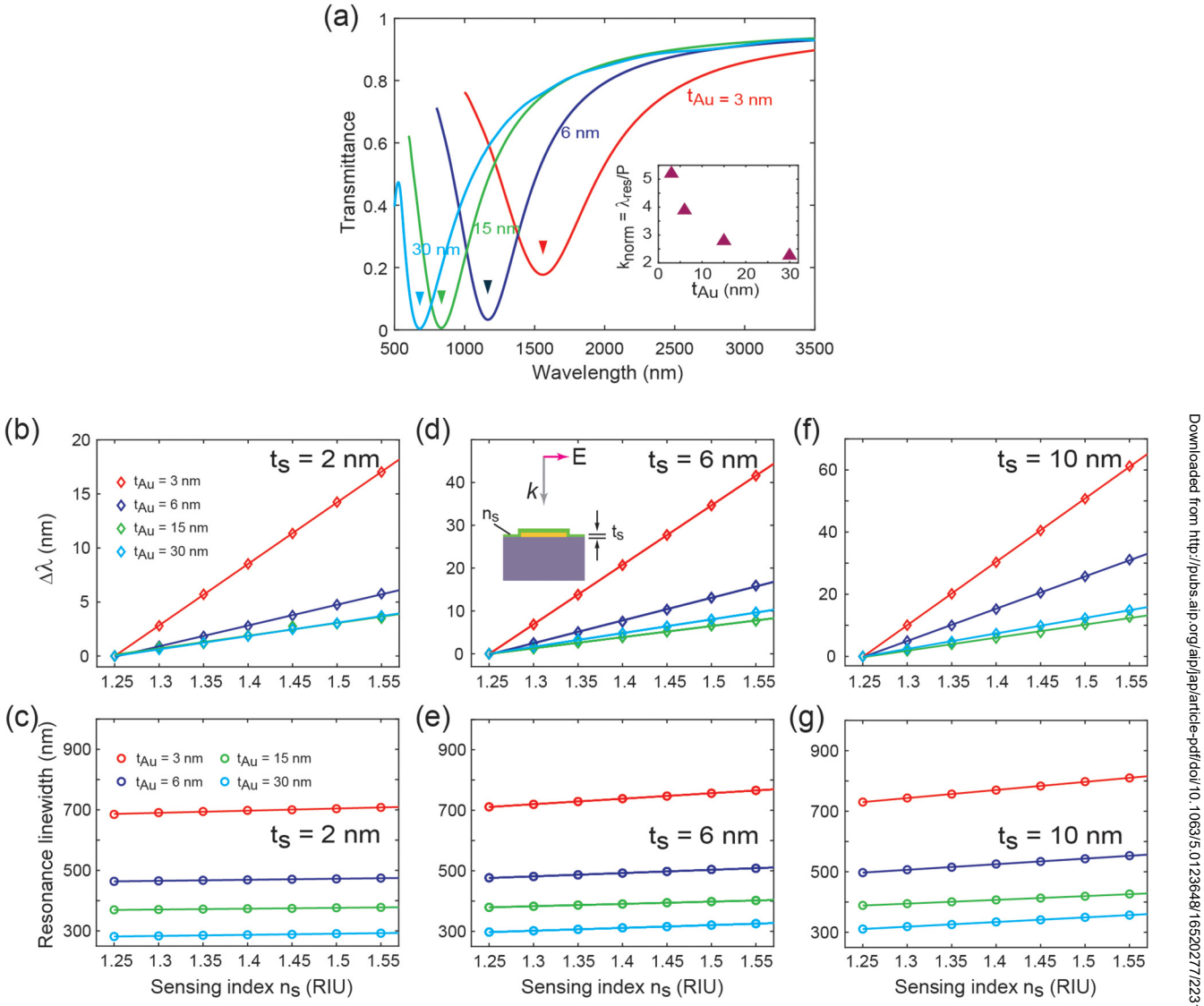

FIG. 3. The influence of thickness-dependent plasmons in ultrathin Au films. (a) The transmittance spectra of Au nanoribbons ($W = 200$ nm, $P = 1.5\,W$) for different thicknesses ($t_{Au} = 3$, 6, 15, and 30 nm). Inset shows the normalized wavenumber of the corresponding resonances as a function of t_{Au}. (b) The resonance wavelength change ($\Delta\lambda$) and (c) resonance linewidth as a function of n_s for systems with different t_{Au} when $t_s = 2$ nm. (d) and (e) The same as panels (c) and (d) but for $t_s = 6$ nm. (f) and (g) The same as panels (c) and (d) but for $t_s = 10$ nm. Results of $t_{Au} = 3$ and 30 nm (Fig. 1) are also presented for comparison purposes.

2D-Ga and 2D-In are treated as homogeneous and isotropic thin films with a thickness of 0.52 and 0.49 nm, respectively. To ensure that the sensors operate in wavelength ranges away from the high optical loss regions,[42] we consider 30 nm-wide 2D-Ga and 50 nm-wide 2D-In nanoribbons (see the supplementary material for details).

Figures 4(a) and 4(b) illustrate the transmittance spectra of the 2D-Ga and the 2D-In devices for RI sensing when $t_s = 10$ nm and n_s vary in a range from 1.25 to 1.55. Resonance wavelength changes of 130 and 190 nm are observed, respectively, which are approximately 2 and 3 times larger than that seen in the 3 nm-Au system discussed previously under the same sensing condition. These observations can be attributed to the strong dispersion of the plasmonic resonances in the 2D-Ga and 2D-In nanoribbons, i.e., $k_{norm}^{2D-Ga} = 59$ and $k_{norm}^{2D-In} = 52$. Figures 4(c) and 4(d) depict the field distributions of the two systems (without the analyte layer) at their resonance wavelength denoted by the dip in the transmittance spectra (gray-dashed curve) shown in Figs. 4(a) and 4(b). A strong

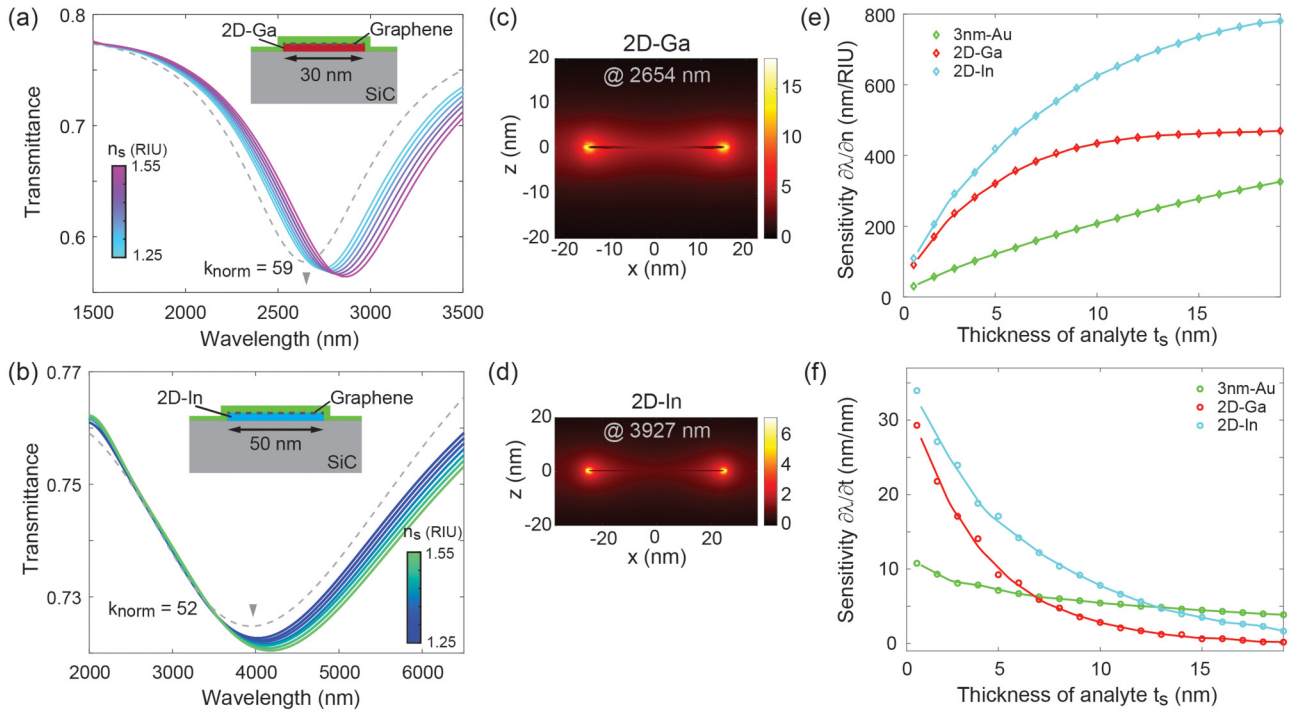

FIG. 4. Ultra-sensitive mid-infrared refractive index sensing based on plasmons in 2D polar metals. (a) Transmittance spectra corresponding to 2D-Ga nanoribbons (W = 30 nm, P = 1.5W) for RI sensing (t_s = 10 nm). (b) Transmittance spectra corresponding to 2D-In nanoribbons (W = 50 nm, P = 1.5W) for RI sensing (t_s = 10 nm). Spectra of both systems without the analyte coating are shown as dashed curves. The insets of (a) and (b) show the schematics of a unit cell of the 2D-Ga and 2D-In nanoribbons for refractive index sensing, respectively. The 2D-Ga and 2D-In films are located on top of a SiC substrate and capped *in situ* with graphene. The corresponding electric field distributions on a cross-sectional plane at a resonance wavelength of (c) 2654 and (d) 3927 nm. The dependence of (e) RI sensitivity $\partial\lambda/\partial n$ and (f) thickness sensitivity $\partial\lambda/\partial t$ on the thickness of the analyte (t_s). For comparison, the results for a 3 nm-Au system are also presented in (e) and (f).

field confinement along with a maximum field enhancement factor of ∼18 is observed in the 2D-Ga nanoribbons, while the 2D-In nanoribbons show a less confined field distribution. This difference in the field concentration primarily arises from the larger material loss of 2D-In at the resonance wavelength (see the supplementary material for the permittivity of 2D-Ga and 2D-In). Nevertheless, we emphasize that the field confinement effect identified in the 2D-In system is still much stronger than that seen in 3 nm-Au nanoribbons [Fig. 1(c)]. These characteristics in the local-field effects determine the RI sensing performances of the discussed 2D-metal sensors. In Figs. 4(e) and 4(f), by presenting the RI sensitivity ($\partial\lambda/\partial n_s$) and thickness sensitivity ($\partial\lambda/\partial t_s$), we provide a comprehensive comparison between the three systems for RI sensing. In the studied range of t_s, both the 2D-Ga and the 2D-In systems show better RI sensitivity than the 3 nm-Au nanoribbons. In particular, a RI sensitivity up to 90 (110 nm/RIU) is observed in the 2D-Ga (2D-In) nanoribbons when covered by a 1 nm-thick analyte layer. On the other hand, as depicted in Fig. 4(f), the strong confinement effect in the studied 2D polar metals also determines the thickness sensitivity of the sensors: the 2D-Ga (2D-In) sensor exhibits $\partial\lambda/\partial t_s$ which is superior to that of the 3 nm-Au nanoribbons when t_s is smaller than ∼7 (∼13 nm).

III. DISCUSSION

Although the thickness (t_M) of a metallic film (with 3D free electron density n_B) needs to satisfy the condition $n_B t_M \ll 1$ to realize a 2D electron gas, pronounced electrical-gating effects have been demonstrated in 3 nm-Au nanostructures.[3] The reported electrically controlled plasmons indicate the potential of 2D-metal optical devices for sophisticated sensing functionalities, such as frequency-selective protein detection, vibrational fingerprints detection, etc., which have been previously achieved using graphene-based mid-infrared biosensors.[35] Furthermore, beyond the three types of 2D-metals considered in our discussion above, the CHet approach can be expanded to encompass a broad set of elements, including but not limited to silver (Ag),[48,49] copper (Cu), zinc (Zn), aluminum (Al), etc., thereby enabling plasmonic sensors based on the entire periodic table of 2D-metals.[50] Furthermore, in practical applications such as sensing of biomolecules, additional processes (e.g., surface engineering) are needed to allow analyte capturing.[51] Moreover, as the field confinement and enhancement are closely dependent on the thickness of the 2D-metals, one may be required to balance the field localization effect and the potential RI sensitivity in the sensor designs. For example, compared with 2D-Ga and 2D-In sensors, the 3 nm-Au based system in our study, which

exhibits unsaturated sensitivity up to a 100 nm-thick analyte, may be more suitable for sensing of larger molecules. On the other hand, for applications involving analytes on the order of a few nm thick, the 2D-In sensor can provide better sensing performance.

Infrared spectroscopy is key to the identification of biological and chemical substances which exhibit infrared vibrational fingerprints, whereas the efficiency and sensitivity of infrared detectors are limited by the poor interaction between mid-infrared light (a few micrometers wavelength) and nanometer-size molecules. Therefore, the high sensitivities of the 2D-Ga and 2D-In nanoribbons observed in our study suggest the applications of 2D-metal sensors in the mid-infrared spectral range. On the other hand, as the FOM of a plasmonic sensor is inversely proportional to its resonance linewidth, the relatively broad spectral responses observed in our proof-of-concept studies reveal the low value of the systems' FOM. We note that the FOM of the 2D-metal sensors can be improved by creating high quality (Q) factor resonances. This can be realized by leveraging interference between different modes supported by the metallic nanostructures. For instance, plasmonic sensors supporting Fano resonances have been demonstrated to exhibit narrower spectra and significantly enhanced FOMs.[28–32] Forming bound states in the continuum (BIC) by creating hybrid resonating systems is another possible approach. Azzam *et al.* have demonstrated BICs with extreme Q-factors arising from coupling of plasmon polaritons with photonic modes.[52] Therefore, single-layer structures with well-controlled dimensions, multilayer planar structures, and plasmonic-photonic hybrid structures might be needed to effectively excite the required plasmons in 2D-metals.[32,52,53] The design of 2D-metal sensors with a simultaneously high FOM value and good accessibility to the enhanced optical field can be a challenging engineering task, but also will deepen our understanding of the dimension-induced electron-photon interactions at interfaces of ultrathin metal films. Moreover, given that the 2D-Ga and 2D-In systems considered here include only a few atomic layers in overall thickness, we envision that certain quantum effects may show up in even thinner 2D-metal films. This may lead to interesting quantum sensing phenomena but is beyond the scope of this work.

IV. CONCLUSIONS

In summary, we have demonstrated that 2D-metal nanostructures supporting plasmonic resonances can be used for resonantly enhanced refractive index sensing. Compared with plasmonic sensors based on conventional metal films, 2D-metal sensors exhibit significantly higher sensitivity of plasmon resonances to changes in their dielectric environment. This can be attributed to the strong electric field confinement and enhancement effect at the surface of 2D-metals due to the strong plasmonic dispersion induced by the thickness effect. Our study shows that the superior sensing performances observed in 2D-metal nanostructures are not only dependent on their thickness but also on the type of metal elements. Given the recent advancements in producing and nanoengineering large-area ultrathin 2D-metal films, it is expected that this work will pave the way for the development of a new family of 2D-metal-based plasmonic devices for sensing applications.

SUPPLEMENTARY MATERIAL

See the supplementary material for optical properties of the 2D-metals used, a comparison of representative plasmonic RI sensors, and the additional simulation results of the proposed sensors.

ACKNOWLEDGMENTS

This work was funded by the DARPA EXTREME program under Award No. HR00111720032. This work was also supported by the National Science Foundation (No. NSF DMR-2002651) and the Penn State MRSEC, Center for Nanoscale Science, under Award No. NSF DMR-2011839.

AUTHOR DECLARATIONS

Conflict of Interest

The authors have no conflicts to disclose

Author Contributions

Lei Kang: Conceptualization (lead); Data curation (lead); Investigation (lead); Methodology (lead); Software (lead); Validation (lead); Visualization (lead); Writing – original draft (lead). **Joshua A. Robinson:** Funding acquisition (equal); Investigation (supporting); Methodology (supporting); Project administration (supporting); Supervision (equal); Writing – original draft (supporting). **Douglas H. Werner:** Funding acquisition (equal); Project administration (equal); Supervision (lead); Writing – original draft (supporting).

DATA AVAILABILITY

The data that support the findings of this study are available from the corresponding author upon reasonable request.

REFERENCES

[1]L. Britnell, R. M. Ribeiro, A. Eckmann, R. Jalil, B. D. Belle, A. Mishchenko, Y.-J. Kim, R. V. Gorbachev, T. Georgiou, S. V. Morozov, A. N. Grigorenko, A. K. Geim, C. Casiraghi, A. H. C. Neto, and K. S. Novoselov, Science **340**, 1311 (2013).
[2]Z. M. Abd El-Fattah, V. Mkhitaryan, J. Brede, L. Fernández, C. Li, Q. Guo, A. Ghosh, A. R. Echarri, D. Naveh, F. Xia, J. E. Ortega, and F. J. García de Abajo, ACS Nano **13**, 7771 (2019).
[3]R. A. Maniyara, D. Rodrigo, R. Yu, J. Canet-Ferrer, D. S. Ghosh, R. Yongsunthon, D. E. Baker, A. Rezikyan, F. J. García de Abajo, and V. Pruneri, Nat. Photonics **13**, 328 (2019).
[4]F. H. da Jornada, L. Xian, A. Rubio, and S. G. Louie, Nat. Commun. **11**, 1013 (2020).
[5]F. F. Zhu, W. J. Chen, Y. Xu, C. L. Gao, D. D. Guan, C. H. Liu, D. Qian, S.-C. Zhang, and J. F. Jia, Nat. Mater. **14**, 1020 (2015).
[6]M. N. Gjerding, M. Pandey, and K. S. Thygesen, Nat. Commun. **8**, 15133 (2017).
[7]Y. Zang, T. Jiang, Y. Gong, Z. Guan, C. Liu, M. Liao, K. Zhu, Z. Li, L. Wang, W. Li, C. Song, D. Zhang, Y. Xu, K. He, X. Ma, S.-C. Zhang, and Q.-K. Xue, Adv. Funct. Mater. **28**, 1802723 (2018).
[8]M. Liao, Y. Zang, Z. Guan, H. Li, Y. Gong, K. Zhu, X.-P. Hu, D. Zhang, Y. Xu, Y.-Y. Wang, K. He, X.-C. Ma, S.-C. Zhang, and Q.-K. Xue, Nat. Phys. **14**, 344 (2018).

[9]R. Sundararaman, T. Christensen, Y. Ping, N. Rivera, J. D. Joannopoulos, M. Soljačić, and P. Narang, Phys. Rev. Mater. **4**, 074011 (2020).
[10]J. Dryzek and A. Czapla, Phys. Rev. Lett. **58**, 721 (1987).
[11]H. Qian, Y. Xiao, and Z. Liu, Nat. Commun. **7**, 13153 (2016).
[12]L. Martín-Moreno, F. J. García-Vidal, H. J. Lezec, K. M. Pellerin, T. Thio, J. B. Pendry, and T. W. Ebbesen, Phys. Rev. Lett. **86**, 1114 (2001).
[13]C. Genet and T. W. Ebbesen, Nature **445**, 39 (2007).
[14]X. Liu, T. Starr, A. F. Starr, and W. J. Padilla, Phys. Rev. Lett. **104**, 207403 (2010).
[15]C. M. Watts, X. Liu, and W. J. Padilla, Adv. Mater. **24**, OP98 (2012).
[16]J. K. Gansel, M. Thiel, M. S. Rill, M. Decker, K. Bade, V. Saile, G. von Freymann, S. Linden, and M. Wegener, Science **325**, 1513 (2009).
[17]Y. Zhao, M. A. Belkin, and A. Alù, Nat. Commun. **3**, 870 (2012).
[18]M. Lapine, I. V. Shadrivov, and Y. S. Kivshar, Rev. Mod. Phys. **86**, 1093 (2014).
[19]G. Li, S. Zhang, and T. Zentgraf, Nat. Rev. Mater. **2**, 17010 (2017).
[20]A. Krasnok, M. Tymchenko, and A. Alù, Mater. Today **21**, 8 (2018).
[21]P. L. Stiles, J. A. Dieringer, N. C. Shah, and R. P. Van Duyne, Annual Rev. Anal. Chem. **1**, 601 (2008).
[22]E. Fort and S. Grésillon, J. Phys. D: Appl. Phys. **41**, 013001 (2008).
[23]E. Petryayeva and U. J. Krull, Anal. Chim. Acta **706**, 8 (2011).
[24]D. Cialla, A. März, R. Böhme, F. Theil, K. Weber, M. Schmitt, and J. Popp, Anal. Bioanal. Chem. **403**, 27 (2012).
[25]J. N. Anker, W. P. Hall, O. Lyandres, N. C. Shah, J. Zhao, and R. P. Van Duyne, Nat. Mater. **7**, 442 (2008).
[26]B. Luk'yanchuk, N. I. Zheludev, S. A. Maier, N. J. Halas, P. Nordlander, H. Giessen, and C. T. Chong, Nat. Mater. **9**, 707 (2010).
[27]T. Weiss, M. Mesch, M. Schäferling, H. Giessen, W. Langbein, and E. A. Muljarov, Phys. Rev. Lett. **116**, 237401 (2016).
[28]S. Zhang, K. Bao, N. J. Halas, H. Xu, and P. Nordlander, Nano Lett. **11**, 1657 (2011).
[29]J. Butet and O. J. F. Martin, Nanoscale **6**, 15262 (2014).
[30]Y. Zhan, D. Y. Lei, X. Li, and S. A. Maier, Nanoscale **6**, 4705 (2014).
[31]F. Hao, Y. Sonnefraud, P. V. Dorpe, S. A. Maier, N. J. Halas, and P. Nordlander, Nano Lett. **8**, 3983 (2008).
[32]M. Mesch, T. Weiss, M. Schäferling, M. Hentschel, R. S. Hegde, and H. Giessen, ACS Sens **3**, 960 (2018).
[33]F. Neubrech, A. Pucci, T. W. Cornelius, S. Karim, A. García-Etxarri, and J. Aizpurua, Phys. Rev. Lett. **101**, 157403 (2008).
[34]M. Golosovsky, V. Lirtsman, V. Yashunsky, D. Davidov, and B. Aroeti, J. Appl. Phys. **105**, 102036 (2009).
[35]D. Rodrigo, O. Limaj, D. Janner, D. Etezadi, F. J. García de Abajo, V. Pruneri, and H. Altug, Science **349**, 165 (2015).
[36]D. Garoli, D. Mosconi, E. Miele, N. Maccaferri, M. Ardini, G. Giovannini, M. Dipalo, S. Agnoli, and F. De Angelis, Nanoscale **10**, 17105 (2018).
[37]V. Faramarzi, V. Ahmadi, M. T. Hwang, and P. Snapp, Biomed. Opt. Express **12**, 4544 (2021).
[38]A. Bolotsky, D. Butler, C. Dong, K. Gerace, N. R. Glavin, C. Muratore, J. A. Robinson, and A. Ebrahimi, ACS Nano **13**, 9781 (2019).
[39]D. Tyagi, H. Wang, W. Huang, L. Hu, Y. Tang, Z. Guo, Z. Ouyang, and H. Zhang, Nanoscale **12**, 3535 (2020).
[40]A. J. Watson, W. Lu, M. H. D. Guimarães, and M. Stöhr, 2D Mater. **8**, 032001 (2021).
[41]B. Wang, Y. Gu, L. Chen, L. Ji, H. Zhu, and Q. Sun, Nanotechnology **33**, 252001 (2022).
[42]K. Nisi, S. Subramanian, W. He, K. A. Ulman, H. El-Sherif, F. Sigger, M. Lassaunière, M. T. Wetherington, N. Briggs, J. Gray, A. W. Holleitner, N. Bassim, S. Y. Quek, J. A. Robinson, and U. Wurstbauer, Adv. Funct. Mater. **31**, 2005977 (2021).
[43]Y. Sun and X. Fan, Opt. Express **16**, 10254 (2008).
[44]Y. Liu, S. Wang, P. Biswas, P. Palit, W. Zhou, and Y. Sun, Sci. Rep. **9**, 1 (2019).
[45]N. Briggs, Z. M. Gebeyehu, A. Vera, T. Zhao, K. Wang, A. De La Fuente Duran, B. Bersch, T. Bowen, K. L. Knappenberger, and J. A. Robinson, Nanoscale **11**, 15440 (2019).
[46]N. Briggs, B. Bersch, Y. Wang, J. Jiang, R. J. Koch, N. Nayir, K. Wang, M. Kolmer, W. Ko, A. De La Fuente Duran, S. Subramanian, C. Dong, J. Shallenberger, M. Fu, Q. Zou, Y.-W. Chuang, Z. Gai, A.-P. Li, A. Bostwick, C. Jozwiak, C.-Z. Chang, E. Rotenberg, J. Zhu, A. C. T. van Duin, V. Crespi, and J. A. Robinson, Nat. Mater. **19**, 637 (2020).
[47]M. A. Steves, Y. Wang, N. Briggs, T. Zhao, H. El-Sherif, B. M. Bersch, S. Subramanian, C. Dong, T. Bowen, M. Lassaunière, V. H. Crespi, J. Robinson, and K. L. Knappenberger, Jr., Nano Lett. **20**, 8312 (2020).
[48]P. Rosenzweig and U. Starke, Phys. Rev. B **101**, 201407 (2020).
[49]W. Lee, Y. Wang, H. Kim, M. Liu, T. N. Nunley, R. Maniyara, C. Dong, J. A. Robinson, V. Crespi, A. H. MacDonald, and C.-K. Shih, arXiv, 2011.01914 (2020).
[50]Y. Wang and V. H. Crespi, Phys. Rev. B **101**, 201407(R) (2020).
[51]A. M. Shrivastav, U. Cvelbar, and I. Abdulhalim, Commun. Biol. **4**, 70 (2021).
[52]S. I. Azzam, V. M. Shalaev, A. Boltasseva, and A. V. Kildishev, Phys. Rev. Lett. **121**, 253901 (2018).
[53]S. Lan, S. P. Rodrigues, M. Taghinejad, and W. Cai, Laser Photonics Rev. **11**, 1600312 (2017).